Cosmological perturbations in a generalised axion-like dark energy model

Carlos G. Boiza[1, a] and Mariam Bouhmadi-López[2, 1, b]

[1]*Department of Physics & EHU Quantum Center,*
University of the Basque Country UPV/EHU, P.O. Box 644, 48080 Bilbao, Spain
[2]*IKERBASQUE, Basque Foundation for Science, 48011, Bilbao, Spain*

We analyse the cosmological evolution of a generalised axion-like field that drives the late-time acceleration of the Universe. This model can exhibit tracking behaviour which alleviates the coincidence problem. The cosmological perturbations are carried within a multi-fluid approach where the scalar field is described by a non-adiabatic fluid, i.e., whose speed of sound at the rest frame is different from the adiabatic one. The cosmological perturbations are solved since the radiation-dominated epoch and imposing initial adiabatic conditions for matter, radiation and the dark energy component, for modes well outside the Hubble horizon in the past. We analyse the homogeneous curvature perturbation, gravitational potential and dark energy perturbations in this model, as well as the matter power spectrum and $f\sigma_8$. We discuss which parameters of the model are more favoured observationally.

I. INTRODUCTION

In recent years, experiments have detected and confirmed a late-time accelerated expansion of the Universe [1–3]. The nature of this acceleration remains unknown. The simplest way to include such accelerated expansion in a cosmological model is through the introduction of a cosmological constant, leading to the ΛCDM model. Although this model successfully explains most observations, it presents some unresolved issues. On the one hand, at a fundamental level, the cosmological constant introduces a new energy scale, $\rho_v \approx 10^{-47}\,\mathrm{GeV}^4$, which is very small compared to other known scales in particle physics [4, 5]. Additionally, the fact that the amounts of matter and dark energy are comparable today, i.e., $\Omega_{m0} \sim \Omega_{de0}$, cannot be explained naturally within this model without fine-tuning the initial conditions. This is known as the coincidence problem [6, 7]. On the other hand, recent observations indicate a tension in determining the current expansion rate H_0 of the Universe. Low-redshift measurements favour higher values of H_0 compared to those obtained through high-redshift measurements [8–10]. A similar tension arises when determining the value of S_8 [11–13]. There is also the so-called neutrino tension: cosmological constraints on the sum of neutrino masses are lower than those obtained through particle physics experiments [14–19]. For all these reasons, models that go beyond the standard ΛCDM cosmological model have been proposed and studied in recent years, from perfect fluids [20–22] to modified theories of gravity [23].

In this work, we focus on a model in which dark energy is described by a scalar field minimally coupled to gravity: a quintessence model. These types of models have proven useful in alleviating the coincidence problem through scaling solutions [24, 25] and tracking behaviour [26, 27].

Specifically, we focus on the generalised axion-like dark energy model, motivated in [28]. In this model, the scalar potential is given by $V(\phi) = \Lambda^4\left[1 - \cos\left(\phi/\eta\right)\right]^{-n}$, where Λ, η and n are free positive parameters, which motivated us to name it generalised axion-like, since the same potential for $n < 0$ naturally appears in axionic models in particle physics (see [29–32] for details on axions applied to cosmology). The potential for $n < 0$ has been previously analysed in the literature: it has been used to attempt to alleviate the coincidence problem through the string axiverse [33, 34], in early dark energy models to address the Hubble tension [9, 10], in Natural Inflation models [35], in primordial black holes formation mechanims [36] and also in axionic dark matter models [37, 38]. Cosmological simulations based on ultralight axions have been performed in [39–41]. In our case, we assume $n > 0$. In [28], we demonstrated how the potential is capable of generating tracking behaviour, allowing us to alleviate the coincidence problem. We also showed how the transition from matter to dark energy can be favoured in this model compared to others. In [42], the authors studied the differences between the generalised axion-like model and an inverse power-law potential and concluded that the former is able to describe the Universe evolution in a more satisfactory way, as the transition from matter to dark energy occurs more rapidly and the equation of state today deviates less from -1.

To study structure formation, one must go beyond the background analysis conducted in [28]. Perturbation theory provides a mathematical framework to analyse the inhomogeneities of the Universe and deduce observable quantities such as the matter power spectrum and the distribution of $f\sigma_8$, thus allowing us to compare the model expected results with observations related to the clustering of matter. Cosmological perturbations have been extensively studied in the literature, including those of a scalar field in quintessence models [43–50]. However, we will show that in this work, it will suffice to adopt a multi-fluid picture, as used in [22], since the cases considered do not involve oscillatory regimes.

The paper is organized as follows. In Sec. II, we will

---

[a] carlos.garciab@ehu.eus
[b] mariam.bouhmadi@ehu.eus

introduce the generalised axion-like model and review its most important aspects, which we have already analysed in depth in [28], such as the tracking behaviour. In Sec. III, we will introduce the cosmological perturbations framework we will use. In Subsec. III A, we will review the general aspects of perturbations in a quintessence model and explain why the multi-fluid picture used in [22] will be sufficient for the cases studied here. In Subsec. III B, we will introduce the adiabatic mode first studied by Weinberg in [51] and the comoving and homogeneous curvature perturbations. In Subsec. III C, we will discuss the initial conditions chosen to numerically solve the perturbation equations in our model. In Sec. IV, we will discuss the numerical results obtained. We will examine the behaviour of the homogeneous curvature perturbation, the gravitational potential and the dark energy perturbation in Subsecs. IV A, IV B and IV C, respectively. In Sec. V, we will study how structure formation operates in our model. We will analyse the matter power spectrum and the $f\sigma_8$ distribution. Finally, in Sec. VI, we will conclude with some key aspects of our work.

II. THE MODEL

In this section, we review the generalised axion-like model and the key aspects of its dynamics. We performed a detailed analysis of it in [28]. The model was proposed to explain the late-time acceleration of the Universe through a scalar field minimally coupled to gravity. It is a quintessence model whose action is given by

$$S = \int d^4x \sqrt{-g} \left(\frac{R}{2k^2} + L_m + L_r + L_\phi \right), \quad (1)$$

where $k^2 = 8\pi G = 1/M_P^2$ (we use natural units $\hbar = c = 1$ throughout this work and $M_P \approx 2.435 \times 10^{18}\,\text{GeV}$ is the reduced Planck mass), R is the scalar curvature, L_m is the Lagrangian corresponding to dark and baryonic matter, L_r is the Lagrangian corresponding to radiation and L_ϕ is the Lagrangian of a minimally coupled scalar field ϕ:

$$L_\phi = -\frac{1}{2} g^{\mu\nu} \partial_\mu \phi \partial_\nu \phi - V(\phi), \quad (2)$$

where $V(\phi)$ is the potential of the scalar field and is given in this model by

$$V(\phi) = \Lambda^4 \left[1 - \cos\left(\phi/\eta\right)\right]^{-n}, \quad (3)$$

where Λ, η and n are free positive parameters of the theory. In [28], we studied the generalised axion-like model in a homogeneous and isotropic spatially flat universe described by the spatially flat FLRW metric:

$$ds^2 = -dt^2 + a^2(t) d\bar{x}^2. \quad (4)$$

Therefore, the equation of motion of the scalar field reads

$$\ddot{\phi} + 3H\dot{\phi} + V_{,\phi} = 0, \quad (5)$$

where a dot stands for derivative with respect to the cosmic time t and $V_{,\phi}$ is the derivative of V with respect to ϕ. The Friedmann equation is given by

$$H^2 = \frac{k^2}{3} \left[\rho_m + \rho_r + \frac{1}{2}\dot{\phi}^2 + V(\phi) \right], \quad (6)$$

where ρ_m and ρ_r are the energy densities of dark and baryonic matter and radiation, respectively. Note that the last two terms of (6) can be identified as the energy density of the scalar field: $\rho_\phi = \dot{\phi}^2/2 + V(\phi)$. For completeness, we also introduce the pressure of the scalar field: $p_\phi = \dot{\phi}^2/2 - V(\phi)$. Another useful quantity that we will use in the perturbation equations (see next section) is the fractional energy density which, for each component A, reads as $\Omega_A = \rho_A/\rho$, where ρ is the total energy density: $\rho = \sum_A \rho_A$.

In [28], we expanded the potential (3) around its minimum and found a non-vanishing constant term which plays the role of an effective cosmological constant:

$$V(\phi) \approx \frac{\Lambda_{\text{eff}}}{k^2} + \frac{1}{2}m^2(\phi - \pi\eta)^2, \quad (7)$$

where $\Lambda_{\text{eff}} = k^2\Lambda^4/2^n$ and $m^2 = n\Lambda^4/(2^{n+1}\eta^2)$. The non-vanishing constant term appeared in the dynamical system as a late-time attractor completely dominated by the potential term of the scalar field, allowing for a late-time de Sitter universe in which the equation of state is -1. In this way, we were able to explain the late-time acceleration of the Universe. In addition to the effective cosmological constant, the potential also includes a mass term fully specified by the parameters of the theory.

A crucial aspect of the model is that it exhibits tracking behaviour. In [28], we argued that for the model to be distinguishable from ΛCDM, we should initially be far from the minimum of the potential, $\phi_i/\eta \ll 1$, as we will next explain.

We start by defining the parameter λ as [27, 52–54]

$$\lambda = -\frac{V_{,\phi}}{kV}. \quad (8)$$

We can write λ as a function of ϕ in our model as [28]

$$\lambda(\phi) = \frac{n}{k\eta} \frac{\sin\left(\phi/\eta\right)}{1 - \cos\left(\phi/\eta\right)}. \quad (9)$$

In terms of λ, the initial condition $\phi_i/\eta \ll 1$ is translated into an initial value that satisfies $\lambda_i \gg 1$. We next define the Γ function as [27, 53, 54]

$$\Gamma = \frac{V V_{,\phi\phi}}{V_{,\phi}^2}. \tag{10}$$

In our model, Γ is given by [28]

$$\Gamma = 1 + \frac{1}{2n} + \frac{n}{2k^2\eta^2\lambda^2}. \tag{11}$$

Since $n > 0$, the Γ function satisfies $\Gamma > 1$. Additionally, in the regime where $\lambda \gg 1$, when we are far from the minimum, Γ is well approximated by a constant expression that only depends on the parameter n:

$$\Gamma \approx 1 + \frac{1}{2n}. \tag{12}$$

Both conditions, $\Gamma > 1$ and $\Gamma \approx const.$, are the necessary conditions that guarantee physically interesting tracking behaviour with $w_\phi < w$, where w is the equation of state of the dominant background fluid, as postulated in [27]. Assuming that the dominant background fluid in the tracking regime is matter, with an equation of state $w = 0$, we showed in [28] that the equation of state of the scalar field in this regime is well approximated by an expression that depends only on the parameter n:

$$w_\phi \approx -\frac{1}{1+n}. \tag{13}$$

In addition to the tracking behaviour, we showed in [28] how the generalised axion-like model is capable of favouring a rapid transition to a dark energy-dominated universe at late-time. In a tracking regime dominated by the background fluid, the density parameter of the scalar field scales with time as $\Omega_\phi \propto t^P$, where P is expressed in terms of Γ as [27]

$$P = \frac{4(\Gamma - 1)}{1 + 2(\Gamma - 1)}. \tag{14}$$

If Γ grows rapidly in the final stage of the tracking regime, a rapid transition from matter to dark energy dominance will occur. In our model, after the tracking regime, the scalar field approaches the minimum of the potential and the convergence toward the de Sitter attractor with $\lambda = 0$ occurs much faster than in the case of an inverse power-law potential [42]. Γ grows rapidly and, with it, Ω_ϕ. Other models with tracking behaviour, such as inverse power-law potentials ϕ^{-n}, where Γ remains constant, do not exhibit this effect. In [42], the authors noted this difference between the inverse power-law potentials and the generalised axion-like model, observing that the equation of state of the latter is closer to -1 nowadays, making it more favourable.

We recall the parameter choices made in [28]. For a critical density today of $\rho_c \sim 10^{-47}\,\mathrm{GeV}^4$ ($H_0 \sim$ $10^{-33}\,\mathrm{eV}$), assuming that the Universe is dominated by the potential part of the scalar field near the minimum, we deduce from (7) that $\Lambda_{\mathrm{eff}}/k^2 \sim 10^{-47}\,\mathrm{GeV}^4$. Therefore, $\Lambda^4/2^n$ is fixed: $\Lambda^4/2^n \sim 10^{-47}\,\mathrm{GeV}^4$. In addition, for the scalar field to be rolling close to the minimum by today, we need $m \sim H_0 \sim 10^{-33}\,\mathrm{eV}$, which imposes $\eta^2/n \sim 10^{37}\,\mathrm{GeV}^2$. For $n \sim 1$, both conditions are satisfied if $\Lambda \sim 10^{-3}\,\mathrm{eV}$ and $\eta \sim M_P$. As in [28], we first fix the values of η and n and then calculate the value of Λ by imposing that today the density parameters of matter and radiation are approximately given, respectively, by $\Omega_{m0} = 0.3$ and $\Omega_{r0} = 8 \times 10^{-5}$ ($\Omega_{\phi0}$ is related to the other density parameters through $\Omega_{\phi0} = 1 - \Omega_{m0} - \Omega_{r0}$). Following [28], we fix the parameter η to M_P and consider two different values of the parameter n: $n = 1$ and $n = 0.1$. This parameter choice ensure that we are free of oscillations at the bottom of the potential and that we can use the multi-fluid picture when studying the perturbations (see next section). We find $\Lambda \approx 2.177 \times 10^{-3}\,\mathrm{eV}$ and $\Lambda \approx 2.102 \times 10^{-3}\,\mathrm{eV}$ for the two cases $n = 1$ and $n = 0.1$, respectively.

To conclude this section, we note how the selection of parameters influences the evolution of the scalar field and, consequently, the evolution of the Universe. In [28], we saw how in the case of $n = 1$, there was a suppression of Ω_m due to the difference between $w_\phi \approx -1/2$ in the tracking regime (cf. (13)) and $w_v = -1$, corresponding to a cosmological constant. For the case of $n = 0.1$, the difference is smaller and the suppression is relaxed ($w_\phi \approx -10/11$ in this case). In fact, in the limit $n \to 0$, we recover a flat potential in (3) and the model becomes equivalent to a cosmological constant ($w_\phi \to -1$ in the tracking regime when $n \to 0$). In the following sections, we will explore the effect of this suppression, which depends on the value of n, on the cosmological perturbations and structure formation.

III. COSMOLOGICAL PERTURBATIONS

The cosmological perturbations have been extensively analysed in the literature [43–47]. In this section, we study the linear regime of the perturbations in our model in the Newtonian gauge. We focus on the scalar perturbations and follow an approach similar to the one used in [22].

A. Framework

The perturbed FLRW metric in the Newtonian gauge reads

$$ds^2 = a^2(\eta)[-(1 + 2\Phi(\eta, x^i))d\eta^2 + (1 - 2\Psi(\eta, x^i))d\bar{x}^2], \tag{15}$$

where η is the comoving time, $d\eta = dt/a$, and $\Phi(\eta, x^i)$ and $\Psi(\eta, x^i)$ are the scalar metric perturbations, which

depend on the comoving time and on the spatial coordinates x^i and coincide with the Bardeen potentials [55]. In the absence of anisotropies, the potentials are equal: $\Phi = \Psi$. From now on, we assume that the fluid perturbations do not introduce any anisotropy and that the equality is thus satisfied.

In this work, we follow the multi-fluid approach used in [22]. In this framework, for each fluid A, the evolution equations for the fractional energy density perturbation, $\delta_A = \delta\rho_A/\rho_A$, and the peculiar velocity potential, v_A, are given by [1]

$$\delta'_A = 3(w_A - c_{sA}^2)\delta_A + 3(1 + w_A)\Psi'$$
$$+ (1 + w_A)\left[9\mathcal{H}(c_{sA}^2 - c_{aA}^2) - \frac{\nabla^2}{\mathcal{H}}\right]v_A, \quad (16)$$

$$v'_A = (3c_{sA}^2 - 1)v_A - \frac{c_{sA}^2}{\mathcal{H}(1+w_A)}\delta_A - \frac{\Psi}{\mathcal{H}}, \quad (17)$$

where a prime stands for a derivative with respect to $\log(a/a_0)$, with a_0 being the current value of the scale factor and $\mathcal{H}$ is the conformal Hubble parameter, $\mathcal{H} = aH$. We have introduced the effective and the adiabatic speeds of sound for each fluid A. They respectively read as

$$c_{sA}^2 = \left.\frac{\delta p_A}{\delta\rho_A}\right|_{\text{r.f.}}, \quad c_{aA}^2 = \frac{p'_A}{\rho'_A}. \quad (18)$$

The effective speed of sound is defined in the rest frame (r.f.) of the fluid.

In our model, radiation and matter are described by perfect fluids with constant equations of state of $w_r = 1/3$ and $w_m = 0$, respectively. Both fluids are adiabatic and, since $c_{sA}^2 = c_{aA}^2 = w_A$ for $A = r, m$, (16) and (17) simplify to

$$\delta'_r = \frac{4}{3}\left(\frac{k^2}{\mathcal{H}}v_r + 3\Psi'\right), \quad v'_r = -\frac{1}{\mathcal{H}}\left(\frac{\delta_r}{4} + \Psi\right), \quad (19)$$

$$\delta'_m = \frac{k^2}{\mathcal{H}}v_m + 3\Psi', \quad v'_m = -\left(v_m + \frac{\Psi}{\mathcal{H}}\right). \quad (20)$$

Note that we have performed a Fourier transformation. The equations for each mode are obtained after the substitution $\nabla^2 \to -k^2$ in (16) and (17). From now on, we will work with the Fourier components.

The scalar field perturbations are more complicated but can be accommodated into this multi-fluid picture (see, for example, [48–50]) by making certain assumptions that are satisfied in our model. Perturbing the energy-momentum tensor of the scalar field [2], we find the expressions for the energy density perturbation, the pressure perturbation and the peculiar velocity potential of the scalar field in terms of $\delta\phi$:

$$\delta\rho_\phi = \frac{\mathcal{H}^2}{a^2}\phi'(\delta\phi' - \phi'\Psi) + V_{,\phi}\delta\phi, \quad (21)$$

$$\delta p_\phi = \frac{\mathcal{H}^2}{a^2}\phi'(\delta\phi' - \phi'\Psi) - V_{,\phi}\delta\phi, \quad (22)$$

$$v_\phi = -\frac{\delta\phi}{\mathcal{H}\phi'}. \quad (23)$$

The peculiar velocity (23) is ill-defined if $\phi' = 0$. In that case, the kinetic part of the scalar field is null and the potential term completely dominates. The equation of state of the scalar field becomes $w_\phi = -1$. Note that in the freezing regime, when the scalar field remains almost constant, the equation of state is close to -1 and the potential term dominates over the kinetic part. Nevertheless, this is an approximate regime and, in fact, there is a small evolution that saves us from this problem. The perturbations can be calculated using the variables $\delta_\phi = \delta\rho_\phi/\rho_\phi$ and v_ϕ, as supported by the numerical results obtained in the work and presented in the next section. Another potentially problematic scenario arises if the field is oscillating around the minimum of the potential. In that case, each time the field changes the direction of the oscillation, the derivative of the field becomes null, $\phi' = 0$, and the equation of state takes the value $w_\phi = -1$. This is not an approximate regime and it is really problematic. This framework fails to reproduce finite results and an approach different from the multi-fluid one is needed. In this work, we discuss cases with $\eta = M_P$ in which the field is rolling close to the

---

[1] For each component A, we can write the diagonal components of the perturbed energy-momentum tensor as $\delta T_{A0}^0 = -\delta\rho_A$ and $\delta T_{Aj}^i = \delta p_A \delta_j^i$, where $\delta\rho_A$ and δp_A are, respectively, the perturbation of the energy density and the perturbation of the pressure of the component A. The non-diagonal components will be given by $\delta T_{Ai}^0 = (p_A + \rho_A)\partial_i v_A$, where v_A is the peculiar velocity potential. We note that, since we have assumed we are free of anisotropies, there will be no purely spatial non-diagonal components. The evolution equations (16) and (17) are easily deduced from the perturbed energy-momentum conservation equations for each component A: $\nabla_\mu \delta T_{A\nu}^\mu + \delta\Gamma_{\mu\alpha}^\mu T_{A\nu}^\alpha - \delta\Gamma_{\mu\nu}^\alpha T_{A\alpha}^\mu = 0$, where ∇_μ is constructed from the Christoffel symbol of the background FLRW metric and $\delta\Gamma_{\mu\nu}^\alpha$ is the perturbation of the Christoffel symbol.

[2] The energy-momentum tensor of the scalar field is given by $T_{\mu\nu}^\phi = \partial_\mu\phi\partial_\nu\phi - \frac{1}{2}g_{\mu\nu}g^{\alpha\beta}\partial_\alpha\phi\partial_\beta\phi - g_{\mu\nu}V(\phi)$. The expressions (21), (22) and (23) are obtained by perturbing the tensor and writing it in the same form as in the case of a fluid: $\delta T_{\phi 0}^0 = -\delta\rho_\phi$, $\delta T_{\phi j}^i = \delta p_\phi \delta_j^i$ and $\delta T_{\phi i}^0 = (p_\phi + \rho_\phi)\partial_i v_\phi$.

minimum nowadays and asymptotically reaches the minimum, but it does not cross it, at least at the times computed. Therefore, the fluid approach is sufficient for us. Perturbations in an oscillatory regime ($\eta < M_P$) will be analysed in a work in preparation [56].

In order to define the evolution equations (16) and (17) for the scalar field ($A = \phi$), we need to find the expressions for w_ϕ, $c_{s\phi}^2$ and $c_{a\phi}^2$. The equation of state is given by $w_\phi = p_\phi/\rho_\phi$ and can be written in terms of the background quantities as

$$w_\phi = \frac{\dot{\phi}^2/2 - V(\phi)}{\dot{\phi}^2/2 + V(\phi)}. \tag{24}$$

From (21), (22) and (23), we find the relation

$$\delta p_\phi = \delta\rho_\phi + 2\mathcal{H}\phi' V_{,\phi} v_\phi. \tag{25}$$

We find that the second term on the right hand side is proportional to v_ϕ. Therefore, the scalar field does not behave like an adiabatic fluid. The pressure perturbation of a fluid A can be separated into its adiabatic part and its non-adiabatic part as [57, 58]

$$\delta p_A = c_{aA}^2 \delta\rho_A + \delta p_{naA}. \tag{26}$$

Following [58], and also used in [22], we can express the non-adiabatic part in the Newtonian gauge as

$$\delta p_{naA} = (c_{sA}^2 - c_{aA}^2)(\delta\rho_A + \mathcal{H}\rho_A' v_A). \tag{27}$$

Introducing the last expression into (26), we finally obtain [3]

$$\delta p_A = c_{sA}^2 \delta\rho_A - 3\mathcal{H}(c_{sA}^2 - c_{aA}^2)(1 + w_A)\rho_A v_A. \tag{28}$$

Comparing (28) for a general fluid with the relation (25) valid for the scalar field, we find the expressions for $c_{s\phi}^2$ and $c_{a\phi}^2$ in terms of the background components:

$$c_{s\phi}^2 = 1, \quad c_{a\phi}^2 = 1 + \frac{2a^2 V_{,\phi}}{3\mathcal{H}^2\phi'}. \tag{29}$$

Note that, again, the adiabatic speed of sound is ill-defined if $\phi' = 0$. With this, we have expressed w_ϕ, $c_{s\phi}^2$ and $c_{a\phi}^2$ in terms of the background quantities. Therefore, (16) and (17) are well defined for the scalar field and the multi-fluid approach is valid if $\phi' = 0$ is not reached.

---

[3] We have used the background conservation equation, given by $\rho_A' + 3(1 + w_A)\rho_A = 0$, to eliminate ρ_A' in (28).

In addition to the evolution equations of δ_A and v_A for each component A, we also have the perturbed Einstein equations, which read as [22, 47]

$$\Psi' + \left(1 + \frac{k^2}{3\mathcal{H}^2}\right)\Psi = -\frac{\delta}{2}, \tag{30}$$

$$\Psi' + \Psi = -\frac{3}{2}\mathcal{H}v(1 + w_{\text{eff}}), \tag{31}$$

$$\Psi'' + \left[3 - \frac{1}{2}(1 + 3w_{\text{eff}})\right]\Psi' - 3w_{\text{eff}}\Psi = \frac{3}{2}\frac{\delta p}{\rho}, \tag{32}$$

where we have introduced the total fractional energy density perturbation, the total pressure perturbation, the total equation of state and the total peculiar velocity potential, which respectively read

$$\delta = \sum_A \Omega_A \delta_A, \quad \delta p = \sum_A \delta p_A,$$
$$w_{\text{eff}} = \sum_A \Omega_A w_A, \quad v = \sum_A \frac{1 + w_A}{1 + w_{\text{eff}}}\Omega_A v_A. \tag{33}$$

B. Adiabatic mode and comoving and homogeneous curvature perturbations

In this subsection, we review the adiabatic mode as introduced by Weinberg in [51], and also studied in [59]. This will be helpful to explain some of our results discussed in the following sections.

In the Newtonian gauge, in the limit of vanishing wave number, $k/\mathcal{H} \to 0$, there is an extra gauge freedom given by a redefinition of the cosmic time and a rescaling of the spatial coordinate:

$$t \to t + \epsilon(t), \quad x^i \to (1 - \theta)x^i, \tag{34}$$

where $\epsilon(t)$ is an arbitrary infinitesimal function of the time and θ is an arbitrary infinitesimal constant. It can be shown that, in this limit, there is a physical solution which can be completely expressed in terms of the gauge transformation [51]:

$$\Psi = H\epsilon - \theta,$$
$$\delta\rho = -\epsilon\dot{\rho}, \quad \delta p = -\epsilon\dot{p}, \quad \delta\rho_A = -\epsilon\dot{\rho}_A, \quad \delta p_A = -\epsilon\dot{p}_A,$$
$$av = \epsilon, \quad av_A = \epsilon, \tag{35}$$

where we have introduced the total background pressure, $p = \sum_A p_A$. In absence of an anisotropic stress tensor, as in our case, the gauge transformations ϵ and θ are related [51]:

$$\epsilon(t) = \frac{\theta}{a(t)} \int^t a(t') dt', \qquad (36)$$

with an arbitrary lower limit.

In a universe dominated by a fluid B with constant equation of state w_B, the scale factor satisfies a power-law time dependence, $a \propto t^{2/[3(1+w_B)]}$, and the Hubble parameter is given by $H = \dot{a}/a = 2/[3t(1+w_B)]$. With this, the dominant part of (36) reads

$$\epsilon = \frac{2\theta}{H(5+3w_B)}. \qquad (37)$$

Taking into consideration this relation and the conservation equations for each component, $\dot{\rho}_A = -3H(1+w_A)\rho_A$, the physical solution given by (35) can be rewritten as

$$\Psi = -\frac{3\theta(1+w_B)}{5+3w_B},$$
$$\frac{\delta}{3(1+w_{\text{eff}})} = \frac{\delta_A}{3(1+w_A)} = \frac{2\theta}{5+3w_B}, \qquad (38)$$
$$\mathcal{H}v = \mathcal{H}v_A = \frac{2\theta}{5+3w_B},$$

where we have eliminated the pressure relations since they are redundant [4].

On the other hand, the comoving curvature perturbation is defined as [55]

$$\mathcal{R} = -\Psi + \mathcal{H}v. \qquad (39)$$

It can be shown that this mode is conserved in the super-Hubble regime $k/\mathcal{H} \ll 1$ if and only if the total perturbation is adiabatic: $\delta\rho/\dot{\rho} = \delta p/\dot{p}$. Of course, the adiabatic mode satisfies this condition and $\mathcal{R}$ is conserved. In fact, from (38) we find that, in a universe dominated by a single fluid, the comoving curvature perturbation is given by $\mathcal{R} = \theta$. It is equally important to introduce the homogeneous curvature perturbation, which is defined as [60]

$$\zeta = -\Psi - \delta\rho/\rho'. \qquad (40)$$

It is sometimes used instead of $\mathcal{R}$ since, in the super-Hubble limit $k/\mathcal{H} \to 0$, the two perturbed quantities coincide [5].

————————

[4] Note that, if $\delta\rho_A = -\epsilon\dot{\rho}_A$ and $av_A = \epsilon$, $\delta p_{naA}=0$, as can be deduced from (27). Therefore, (26) simplifies to $\delta p_A = c_{aA}^2 \delta\rho_A$, where $c_{aA}^2 = \dot{p}_A/\dot{\rho}_A$ (cf. (18)), and, since $\delta\rho_A = -\epsilon\dot{\rho}_A$, we find $\delta p_A = -\epsilon\dot{p}_A$.

[5] As noted in [61], $\delta\rho/\rho' \to -\mathcal{H}v$ in the limit $k/\mathcal{H} \to 0$. Therefore, $\zeta \to \mathcal{R}$ in the limit $k/\mathcal{H} \to 0$.

C. Initial conditions

In order to solve numerically the perturbation equations, we must impose initial conditions. We assume that, initially, the Universe is dominated by the radiation component. We set the initial time at $\log(a_i/a_0) = -15$. Therefore, we have initially $\rho_i \approx \rho_{ri}$, $\delta_i \approx \delta_{ri}$, $\delta p_i \approx \delta p_{ri}$, $w_{\text{eff}i} \approx 1/3$ and $v_i \approx v_{ri}$. At this moment, all the relevant modes in the linear regime are super-Hubble and their wave number are much smaller than the comoving Hubble parameter, $k \ll \mathcal{H}$. Combining (30) and (32), we obtain in this initial stage that the dominant solution is given by a constant metric potential, $\Psi \approx const.$ [22, 47]. For this reason, we impose $\Psi'_i = 0$. Therefore, from (30) and (31), we deduce that initially the perturbations must satisfy

$$\Psi_i = -\frac{\delta_i}{2[1+k^2/(3\mathcal{H}_i^2)]},$$
$$\Psi_i = -\frac{3}{2}\mathcal{H}_i v_i(1+w_{\text{eff}i}). \qquad (41)$$

We have included the term $(k/\mathcal{H}_i)^2$ despite the fact that, initially, we are in the super-Hubble regime. This is necessary so that Ψ'_i is exactly zero at the starting point of the simulations. If we eliminate this term, some small oscillations happen at the beginning, but a fast convergence to $\Psi' = 0$ is reached. In addition, motivated by single scalar field models of inflation, we choose adiabatic initial conditions, which read as [22, 62]

$$\frac{3\delta_{ri}}{4} = \delta_{mi} = \frac{\delta_{\phi i}}{1+w_{\phi i}} = \frac{\delta_i}{1+w_{\text{eff}i}}, \qquad (42)$$
$$v_{ri} = v_{mi} = v_{\phi i} = v_i.$$

All together, from (41) and (42) we find that, initially, the perturbations must satisfy

$$\frac{3\delta_{ri}}{4} = \delta_{mi} = \frac{\delta_{\phi i}}{1+w_{\phi i}} = \frac{\delta_i}{1+w_{\text{eff}i}} = -\frac{2[1+k^2/(3\mathcal{H}_i^2)]\Psi_i}{1+w_{\text{eff}i}},$$
$$v_{ri} = v_{mi} = v_{\phi i} = v_i = -\frac{2\Psi_i}{3(1+w_{\text{eff}i})\mathcal{H}_i}. \qquad (43)$$

Note that the initial conditions are consistent with the relations in (38) in a universe initially dominated by radiation, $w_{\text{eff}i} \approx w_B = 1/3$. In fact, the adiabatic mode is dominant until modes become sub-Hubble.

The comoving curvature perturbation (39) is conserved for super-Hubble modes if the perturbation is adiabatic, $\delta\rho/\dot{\rho} = \delta p/\dot{p}$, as discussed in the previous subsection. Initially, since the Universe is dominated by radiation and $k \ll \mathcal{H}$, $\mathcal{R}$ is conserved. In fact, $\mathcal{R}$ is also conserved after the transition to matter until the mode enters the horizon. In the asymptotic future, when the Universe is dominated by the scalar field, the modes become super-Hubble again. Moreover, the perturbation also become

adiabatic and $\mathcal{R}$ is conserved again, as we will see in detail in the next section.

As was done in [22], we set $\Psi_i = 1$ to perform the numerical calculations. After solving the equations, we rescale the solution by taking into account the physical value of $\delta_{\text{phys}}(k)$, whose value is inferred from the Planck observational fit to single field inflation [63]:

$$\delta_{\text{phys}}(k) = \frac{2\pi}{3} \sqrt{2A_s} \left(\frac{k}{k_{\text{pivot}}} \right)^{\frac{n_s - 1}{2}} k^{-3/2}, \qquad (44)$$

where A_s and n_s are the scalar amplitude and spectral index of the primordial inflationary power spectrum, respectively, corresponding to a pivot scale k_{pivot}. Here we use $\ln(10^{10} A_s) = 3.0448$, $n_s = 0.96605$ and $k_{\text{pivot}} = 0.05 \text{ Mpc}^{-1}$ [63].

IV.   NUMERICAL RESULTS

In this section, we present the numerical results obtained when solving the perturbation equations discussed in the previous section. As we have shown, the equations for the scalar field perturbations depend on background quantities (cf. (24) and (29)). Therefore, to numerically solve the perturbation equations, we must first solve the dynamical system associated with the background. This system was numerically solved and analysed in our previous work [28].

A.   Homogeneous curvature perturbation

In the previous section we introduced the comoving curvature perturbation, $\mathcal{R}$, and the homogeneous curvature perturbation, ζ (see (39) and (40), respectively). In this work, we focus on ζ, since the two curvature perturbations coincide in the super-Hubble limit $k/\mathcal{H} \to 0$.

In Figs. 1a and 1b, we have represented the evolution of ζ for different modes in the cases $n = 1$ and $n = 0.1$, respectively. Initially, every mode is in the super-Hubble regime, $k/\mathcal{H} \ll 1$, and the adiabatic mode dominates (cf. (35)), so the homogeneous curvature perturbation is conserved. When the modes enter the horizon, the conservation is broken and some non-trivial evolution happens. We see that, in the far future, the homogeneous curvature perturbation is conserved again. In the final stage, the scalar field dominates and all of the modes exit the Hubble horizon and become super-Hubble again. $\mathcal{R}$ and ζ coincide in the super-Hubble limit because $\delta\rho/\rho' \to -\mathcal{H}v$ as $k/\mathcal{H} \to 0$ [61]. Since the scalar field dominates at late-time, we find from (27) that the non-adiabatic part vanishes for super-Hubble modes and the perturbation becomes adiabatic [6]. Therefore, ζ is conserved again.

Note that the relations in (35) are not generally satisfied in the final stage. Even so, the super-Hubble regime and the adiabaticity of the total perturbation guarantee the conservation of the homogeneous curvature perturbation, as in our case.

B.   Gravitational potential

In the Newtonian gauge, in absence of anisotropies, the scalar metric perturbations Ψ and Φ introduced in (15) coincide: $\Psi = \Phi$. In this case, Ψ plays the role of the gravitational potential.
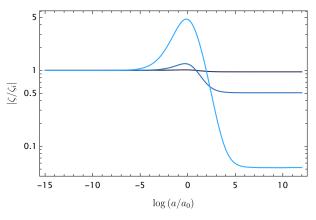
In Figs. 2a and 2b, we have represented the evolution of the gravitational potential for different modes in the cases $n = 1$ and $n = 0.1$, respectively, and we have compared them with the evolution of ΛCDM. Initially, both cases have the same evolution and the differences with respect to a cosmological constant are not appreciable. Every mode is super-Hubble at the beginning of the simulations and the adiabatic mode dominates. Therefore, the gravitational potential remains constant and satisfies the relation given in (38), with $w_B = 1/3$. The modes that cross the horizon in the radiation-dominated era suffer from a strong suppression. In fact, these modes oscillate with frequency $k/\sqrt{3}$ and their amplitudes decrease as a^{-2} in the sub-Hubble regime [47].
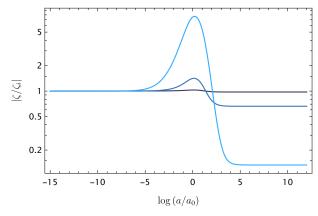
In the matter era, the dominant solution for the gravitational potential is a constant both in the super-Hubble and in the sub-Hubble regimes. Consequently, the modes that enter in the horizon in the matter era only suffer from a suppression due to the transition from radiation to matter. If during the transition the super-Hubble regime is still valid, the adiabatic mode is dominant and the gravitational potential satisfies the relation given in (38), with $w_B = 1/3$ in the radiation era and $w_B = 0$ in the matter era. Therefore, the suppression factor is given by $\Psi_m/\Psi_r = 9/10$, where Ψ_m is the gravitational potential in the matter era and Ψ_r is the gravitational potential in the radiation era. Apart from this suppression, the gravitational potential remains constant once the mode enters the horizon.

The differences with respect to ΛCDM are appreciable only at late-time, in the transition from matter to dark energy. For the case $n = 1$, represented in Fig. 2a, we observe a suppression at low redshift with respect to ΛCDM. As mentioned in [28], in this case the matter component is suppressed in favour of the dark energy component due to tracking far from $w_v = -1$. From (31), we see that $\Psi \to 0$ and $\Psi' \to 0$ asymptotically in

---

[6] Note that, since in the final stage the scalar field dominates, we
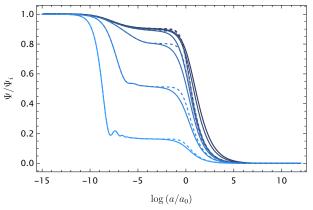
have $\rho \approx \rho_\phi$, $\delta\rho \approx \delta\rho_\phi$ and $v \approx v_\phi$. Since in the final stage all the modes in the linear regime are super-Hubble ($k/\mathcal{H} \ll 1$), we also have $\delta\rho/\rho' \approx -\mathcal{H}v$. Therefore, $\delta\rho_\phi/\rho'_\phi \approx -\mathcal{H}v_\phi$ and the non-adiabatic part of the scalar field vanishes (see (27) for $A = \phi$). It means that the total perturbation is adiabatic, since in this stage $\delta p \approx \delta p_\phi$.
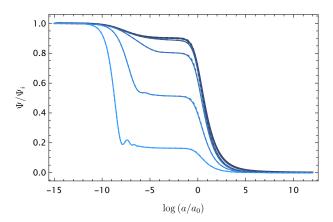
(a) Representation of the evolution of $|\zeta/\zeta_i|$ for n=1.

(b) Representation of the evolution of $|\zeta/\zeta_i|$ for n=0.1.

Figure 1: The left hand side panel shows the evolution of the absolute value of the homogeneous curvature perturbation normalised to its initial value, $|\zeta/\zeta_i|$, for the case $n = 1$. Each colour represents a different mode k of the perturbations. We have represented three different modes: $k = 10^{-4}$h Mpc^{-1} (the last to enter the horizon, represented by dark blue), $k = 4 \times 10^{-4}$h Mpc^{-1} (represented by medium shade of blue) and $k = 1.6 \times 10^{-3}$h Mpc^{-1} (represented by light blue). Note that, for every mode represented, the linear regime is valid ($k < 0.2$h Mpc^{-1}). The right hand side panel shows the evolution of $|\zeta/\zeta_i|$ for the case $n = 0.1$. Each colour represents the same mode as in the left hand side panel. Conservation of the homogeneous curvature perturbation is observed both at the beginning of the simulations, when adiabatic mode dominates, and at very late-time in the future, when the perturbation is in the super-Hubble regime and becomes adiabatic again.

(a) Representation of the evolution of Ψ/Ψ_i for n=1.

(b) Representation of the evolution of Ψ/Ψ_i for n=0.1.

Figure 2: The left hand side panel shows the evolution of the gravitational potential normalised to its initial value, Ψ/Ψ_i, for the case $n = 1$. Each colour represents a different mode k of the perturbations. We have represented six different modes ranging from $k = 10^{-4}$h Mpc^{-1} (the last to enter the horizon, represented by the darkest blue) to $k = 0.1$h Mpc^{-1} (the first to enter the horizon, represented by the lightest blue). Once again, we have selected each mode to ensure it falls within the validity of the linear regime ($k < 0.2$h Mpc^{-1}). The solid lines represent the evolution of the gravitational potential in our model, while the dashed lines represent the evolution in ΛCDM for the same modes. The right hand side panel shows the evolution of Ψ/Ψ_i for the case $n = 0.1$. Each colour represents the same mode as in the left hand side panel. Bigger differences with respect to ΛCDM are observed for the $n = 1$ case, when tracking happens far from $w_v = -1$.

the future when the potential of the scalar field dominates and $w_{\text{eff}} \to -1$. The transition to $\Psi \to 0$ begins earlier if the scalar field acquires importance in the tracking epoch, as happens in this case, since w_ϕ is further from -1. We observe this effect in Fig. 2a. In the case $n = 0.1$, represented in Fig. 2b, tracking occurs closer to $w_v = -1$

and the matter component does not suffer from a big suppression. In this case, the transition to $\Psi \to 0$ at late-time is not accelerated and the differences with respect to ΛCDM are relaxed.

C. Dark energy perturbation

In the previous section, we argued that the multi-fluid picture could be used in this work since we have no oscillatory regime of the scalar field in the cases analysed and $\phi' \neq 0$. In this approach, the perturbations of the scalar field are studied by solving the evolution of $\delta\rho_\phi$ and v_ϕ, defined in (21) and (23), respectively. The scalar field behaves like a non-adiabatic fluid with $c_{s\phi}^2 \neq c_{a\phi}^2$, both defined in (29).

In Figs. 3a and 3b, we have represented the evolution of $\delta_\phi/(1 + w_\phi)$ for different modes in the cases $n = 1$ and $n = 0.1$, respectively (we remind that $\delta_\phi = \delta\rho_\phi/\rho_\phi$). As previously mentioned, the adiabatic mode is the dominant one at the beginning, when every mode is super-Hubble and the Universe is dominated by radiation. In this early evolution, the relations (38) are satisfied with $w_B = 1/3$ and we expect $\delta_\phi/(1 + w_\phi)$ to remain constant, as observed in the figures. The modes that do not enter the horizon during the radiation-dominated era experience an enhancement in the transition to matter-domination by a factor of $6/5$, since $w_B = 0$ in the matter-dominated era. Once the modes enter in the horizon, their non-adiabatic part becomes important and they decouple from the adiabatic mode.

Every mode becomes super-Hubble again in the future and the total perturbation satisfies $\delta\rho/\rho' \approx -\mathcal{H}v$. Since the Universe is now dominated by the scalar field, this implies $\delta\rho_\phi/\rho_\phi' \approx -\mathcal{H}v_\phi$, as we discussed in Subsec. IV A. Therefore, the non-adiabatic part of the perturbation vanishes. After a Fourier transformation, $\nabla^2 \to -k^2$, (16) can be rewritten as

$$
\left(\frac{\delta_A}{1 + w_A}\right)' = \left[9(c_{sA}^2 - c_{aA}^2) + \left(\frac{k}{\mathcal{H}}\right)^2\right]\mathcal{H}v_A + 3(c_{aA}^2 - c_{sA}^2)\frac{\delta_A}{1 + w_A} + 3\Psi'.
$$
(45)

The late-time regime is given by a universe dominated by the potential part of the scalar field ($w_\phi \approx -1$) in the super-Hubble limit ($k \ll \mathcal{H}$) and, therefore, $\Psi \approx 0$, $\Psi' \approx 0$, $\delta\rho_\phi/\rho_\phi' \approx -\mathcal{H}v_\phi$, as noted in Subsecs. IV A and IV B. From (45) applied to $A = \phi$, we find that [7], at late-time, $\delta_\phi/(1 + w_\phi) \approx const$. We observe this behaviour in Figs. 3a and 3b. Since w_ϕ asymptotically decays to -1 in the cases analysed, we deduce that δ_ϕ must also decay asymptotically to 0 with a rate similar to $\dot{w}_\phi$.

---

[7] Note that, again, we have used the conservation equation for the scalar field: $\rho_\phi' + 3(1 + w_\phi)\rho_\phi = 0$. Therefore, $\delta_\phi/(1 + w_\phi) = -3\delta\rho_\phi/\rho_\phi'$ and, if $\Psi' \to 0$ and $\delta\rho_\phi/\rho_\phi' \to -\mathcal{H}v_\phi$ in the super-Hubble limit ($k/\mathcal{H} \to 0$), the right-hand side of (45) vanishes for $A = \phi$.

V. COSMOLOGICAL OBSERVABLES

After the study conducted in the previous section on perturbations in our quintessence model, we now focus on structure formation in this section. We will explore how observables such as the matter power spectrum and the $f\sigma_8$ distribution can impose constraints on the parameters of the models.

In Figs. 4a and 4b, we have represented the evolution of the growth rate function, $f = \delta_m'/\delta_m$ [22, 64], for different modes in our model. We compare them with the ΛCDM estimation, $f_\Lambda \approx \Omega_{\Lambda m}^\gamma$, where $\gamma = 0.55$ [65–67], valid in the sub-Hubble regime $k \gg \mathcal{H}$. Initially, all the modes are super-Hubble and matter perturbations remain almost constant. Therefore, $f \approx 0$ until the modes enter the horizon. Then, perturbations grow and their growth rates reach a common path given by the approximate function $f \approx \Omega_m^\gamma$, where γ is now given by $\gamma = 0.55 + 0.05[1 + w_\phi(z = 1)]$ [66]. Note that this parametrization is a correction for general dark energy models: we recover $\gamma = 0.55$ in ΛCDM since $w_v = -1$ at every redshift. In the sub-Hubble regime, k dependence is lost in the growth function and we can make a comparison between our model predictions and ΛCDM ones. For the case of $n = 1$ represented in Fig. 4a, we observe a suppression with respect ΛCDM at low redshift. As explained in the previous subsection, tracking with $n = 1$ implies an equation of state w_ϕ further from -1. Therefore, matter component is suppressed in favour of dark energy. The same effect was observed for Ω_m in [28]. Note that, in fact, the growth rate of sub-Hubble modes are well approximated by a parametrization which depends on Ω_m: if we found a suppression in Ω_m, it is expected to find it also in f. For the case of $n = 0.1$ represented in Fig. 4b, sub-Hubble modes fit well to the ΛCDM approximation at lower redshift. In this case, w_ϕ in the tracking regime is closer to -1 and Ω_m is less suppressed [28]. Therefore, the differences in f with respect ΛCDM are less appreciable.

The matter power spectrum gives us information on the distribution of matter over various scales in the Universe. In the Newtonian gauge that we have used in this work, it can be expressed as [22]

$$
P = |\delta_m - 3\mathcal{H}v_m|^2 .
$$
(46)

Another important quantity which usually appears in the observational data when studying structure formation is $f\sigma_8$, a combination of the growth structure function f previously represented in Figs. 4a and 4b and σ_8, which measures the root mean square (rms) fluctuation of the matter density field on a scale of $8h^{-1}$ Mpc. The temporal evolution of σ_8 is given by [22, 68]

$$
\sigma_8(z, k_{\sigma_8}) = \sigma_8(0, k_{\sigma_8})\frac{\delta_m(z, k_{\sigma_8})}{\delta_m(0, k_{\sigma_8})},
$$
(47)

(a) Representation of the evolution of
$k^{3/2} \left| \delta_\phi (1 + w_\phi)^{-1} \right|$ for n=1.

(b) Representation of the evolution of
$k^{3/2} \left| \delta_\phi (1 + w_\phi)^{-1} \right|$ for n=0.1.

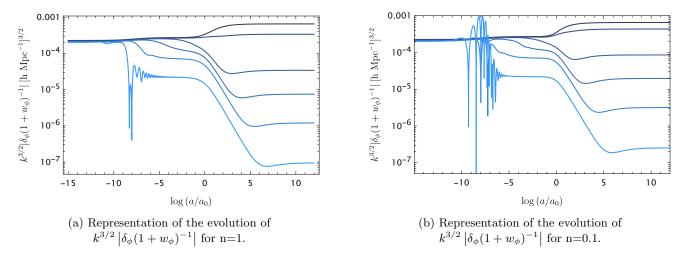Figure 3: The left hand side panel shows the evolution of the scalar field perturbations through the quantity $k^{3/2} \left| \delta_\phi (1 + w_\phi)^{-1} \right|$ for the case $n = 1$. Each colour represents a different mode k of the perturbations. The modes considered and the colour criterion are the same as for Figs. 2a and 2b. The right hand side panel shows the evolution of $k^{3/2} \left| \delta_\phi (1 + w_\phi)^{-1} \right|$ for the case $n = 0.1$. Each colour represents the same mode as in the left hand side panel.
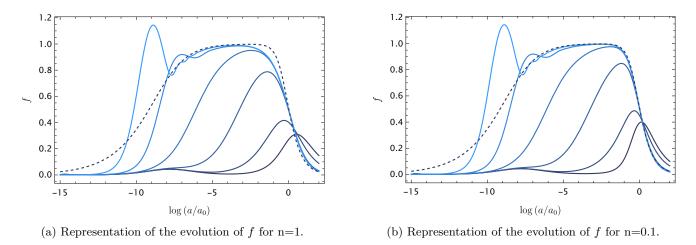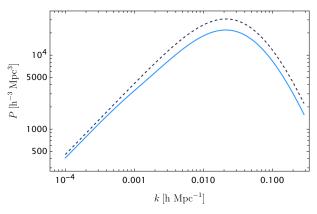

(a) Representation of the evolution of f for n=1.

(b) Representation of the evolution of f for n=0.1.

Figure 4: The left hand side panel shows the evolution of the growth rate function f for $n = 1$. Each colour represents a different mode k of the perturbations. The modes considered and the colour criterion are the same as for Figs. 2a and 2b. The solid lines represent the evolution of the growth rate function in our model, while the dashed line represents the approximation $f_\Lambda \approx \Omega_{\Lambda m}^\gamma$ for ΛCDM, valid in the sub-Hubble regime ($k \gg \mathcal{H}$). The right hand side panel shows the evolution of f for $n = 0.1$. Each colour represents the same mode as in the left hand side panel. Higher suppression with respect to ΛCDM is observed for the $n = 1$ case.

where $k_{\sigma_8} = 0.125$h Mpc^{-1} is the wave-length of the mode corresponding to distances of 8h^{-1} Mpc and we use $\sigma_8(0, k_{\sigma_8}) = 0.8120$ [63].
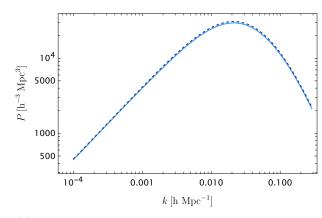
In Figs. 5a and 5b, we have represented the matter power spectrum for $n = 1$ and $n = 0.1$, respectively, at $z = 0$ and we have compared with respect to ΛCDM. As expected, further suppression with respect to ΛCDM is found for $n = 1$ in Fig. 5a, as tracking occurs far from $w_v = -1$. The matter component is suppressed and, as a consequence, structure formation is disfavoured. For $n = 0.1$, represented in Fig. 5b, the difference with respect to ΛCDM is less appreciable. Tracking happens

close to $w_v = -1$ and the matter component evolution mimics the ΛCDM one. Therefore, structure formation is bigger at lower redshift and the suppression of the matter power spectrum is relaxed. In Figs. 5c and 5d, we have represented the temporal evolution of $f\sigma_8$ for $n = 1$ and $n = 0.1$, respectively, in the low redshift range $z \in [0, 2]$. We find the same suppression that was present in Figs. 4a and 4b: for $n = 1$, the deviation from ΛCDM is bigger than for $n = 0.1$.
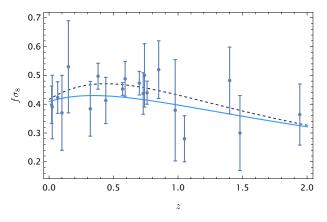
From this section, we find that the structure formation is sensitive to the parameters of the theory. Specifically, having fixed η to the reduced Planck mass, $\eta = M_P$,
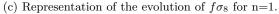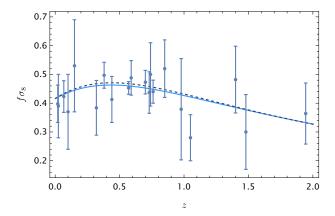
(a) Representation of matter power spectrum for n=1.

(b) Representation of matter power spectrum for n=0.1.

(c) Representation of the evolution of $f\sigma_8$ for n=1.

(d) Representation of the evolution of $f\sigma_8$ for n=0.1.

Figure 5: The top panels show the matter power spectrum from $k = 10^{-4}$h Mpc^{-1} to $k = 0.3$h Mpc^{-1}. Note that the linear regime is valid till $k = 0.2$h Mpc^{-1}; larger values of k have been added in order to better observe the differences of the model with respect to ΛCDM in the high k limit. The solid lines represent the numerical results of the model. The dashed lines represent the ΛCDM estimations. The top-left panel corresponds to the $n = 1$ case, while the top-right panel corresponds to $n = 0.1$. Higher suppression with respect to ΛCDM is observed for the $n = 1$ case. The bottom panels show the evolution of $f\sigma_8$ from redshift $z = 2$ to $z = 0$. The same criterion is used: the solid lines represent the numerical results of the model, while the dashed lines represent the ΛCDM estimations. Observational data have been included in the plots [69]. Again, higher suppression with respect to ΛCDM is observed for the $n = 1$ case (bottom-left panel).

structure formation imposes extra constraints in the parameters. Throughout this work, we have deeply analysed the cases $n = 1$ and $n = 0.1$. We found that both scenarios allow for late-time acceleration in a universe dominated by the dark energy sector today: $\Omega_{m0} \approx 0.3$ and $\Omega_{\phi 0} \approx 0.7$. Observational data on matter structures can help us to further constraint the values of the parameters. The complete evolution of the scalar field plays an important rule, since tracking behaviour allows for scenarios in which the scalar field is not negligible at low redshift and can have appreciable effects in the matter structures which we observe today. In cases in which we are leaving the tracking regime nowadays, as the cases studied here, deviating so much from $w_v = -1$ can be

problematic since we expect big suppression of matter structures with respect to ΛCDM. We have seen this effect by considering the specific cases $n = 1$ and $n = 0.1$.

VI.   CONCLUSIONS

In this work, we first reviewed the generalised axion-like model proposed in [28]. This model arises as a generalisation of the axion-like potential to negative powers (cf. (3)). We have reviewed the most important dynamical aspects of the model, which we discussed in depth in [28]. Specifically, we have shown how the model can explain the late-time acceleration of the Universe through

an effective cosmological constant that comes into play when the scalar field reaches the non-vanishing minimum of the potential (cf. (7)). We have also reviewed how the model exhibits tracking behaviour, which allows for an alleviation of the coincidence problem. Additionally, we have seen that in our model, the transition from matter to dark energy is favoured. This is because Γ (see (10) for a general definition of Γ and (11) for the expression that Γ takes in our model) gets very large when the scalar field reaches the de Sitter-like attractor at $\lambda = 0$. As a result, the amount of dark energy increases sharply in the final phase of the tracking regime (cf. (14)). In [42], the authors noted that this mechanism distinguishes the generalised axion-like model from an inverse power-law potential. In the former, the equation of state today is closer to -1.

After presenting and reviewing the dynamical aspects of the model, we examined the perturbation theory in the linear regime within the Newtonian gauge. We showed that the multi-fluid picture used in [22] is applicable to our quintessence model, as the considered cases ($\eta = M_P$, $n = 1$ & $\eta = M_P$, $n = 0.1$) do not lead to an oscillatory regime for the scalar field; in other words, we avoid points where $\phi' = 0$, at least up to the calculated times. Therefore, the peculiar velocity (23) and the adiabatic speed of sound (29) are well-defined. In the perturbed scalar field equations, some quantities depend on the dynamical evolution of the background (cf. (24) and (29)). Thus, to solve the perturbation equations, we must first solve the background dynamical system, which we have already described in [28].

We have also analysed the adiabatic mode in Subsec. III B, first proposed by Weinberg in [51], and the comoving and homogeneous curvature perturbations (see (39) and (40)), which are conserved in the super-Hubble regime, $k \ll \mathcal{H}$, when the total perturbation is adiabatic. To perform a numerical calculation of the perturbations and observe their evolution, we have imposed adiabatic initial conditions (43), motivated by single-field inflationary models.

After the theoretical introduction to perturbation theory applied to a quintessence model and after selecting the initial conditions, we have conducted a study of the perturbations by numerically solving the equations. This study was carried out for two cases: $\eta = M_P$, $n = 1$ & $\eta = M_P$, $n = 0.1$. First, we have analysed the evolution of the homogeneous curvature perturbation (40), which in the super-Hubble regime, $k \ll \mathcal{H}$, coincides with the comoving curvature perturbation (39). We found that the homogeneous curvature perturbation is conserved at the beginning of the evolution, when we are in the super-Hubble regime and the adiabatic mode (35) dominates. When the modes enter the Hubble horizon, the homogeneous curvature perturbation ceases to be conserved and exhibits a non-trivial evolution. In the future, the Universe is dominated by the scalar field, and the total perturbation becomes adiabatic again. Since the super-Hubble regime is valid once more in this phase,

we find that the homogeneous curvature perturbation is conserved again. It is worth noting that, although the total perturbation becomes adiabatic, the adiabatic mode introduced in Subsec. III B is not recovered in this final stage.

We have also studied the evolution of the gravitational potential for the two cases mentioned above. In both cases, we observe similar behaviour at the beginning. When in the super-Hubble regime and the adiabatic mode dominates, the gravitational potential is constant. Modes that remain in the super-Hubble regime during the radiation-to-matter transition experience a suppression by a factor of $9/10$. Those modes that enter the Hubble horizon before the transition suffer a greater suppression and subsequent oscillation, with a frequency $k/\sqrt{3}$. In the final stage of the evolution, during the matter-to-dark energy transition, the differences between the two cases become apparent. As discussed in [28], the amount of matter undergoes a larger suppression for higher values of the parameter n. Thus, we observe that the transition of the gravitational potential toward $\Psi \to 0$, $\Psi' \to 0$, begins earlier in the case of $n = 1$. For the case $n = 0.1$, the difference from ΛCDM is nearly imperceptible.

We have also analysed the evolution of dark energy perturbations. We found that, initially, when the adiabatic mode dominates and we are in the super-Hubble regime, the quantity $\delta_\phi/(1 + w_\phi)$ remains constant, as expected. When the modes enter the Hubble horizon and the super-Hubble regime is lost, the modes decouple from the adiabatic mode and exhibit non-trivial evolution. By the end of the evolution, we find that the total perturbation, which is approximately given by the dark energy perturbation (since the scalar field dominates), becomes adiabatic again. Since the super-Hubble regime is restored in this final phase, the quantity $\delta_\phi/(1 + w_\phi)$ is conserved once more. Thus, δ_ϕ asymptotically decays toward 0 at the same rate as $\dot{w}_\phi$.

Finally, we have studied the structure formation for the two cases $n = 1$ and $n = 0.1$. The suppression of the parameter Ω_m that we found in [28], which is greater for higher values of n, translates into a suppression in structure formation as compared to ΛCDM. We have observed that in the case of $n = 1$, the suppression of the growth rate function is larger than in the case of $n = 0.1$. We found the same behaviour when studying the matter power spectrum and the $f\sigma_8$ distribution. Therefore, the data we have on structure formation could constrain the values of the parameter n in our model.

To conclude this work, we note that variations in the parameter η could also affect the evolution of the Universe. In fact, values smaller than the reduced Planck mass, $\eta < M_P$, may lead to an oscillatory regime where the perturbations cannot be studied within the multi-fluid framework, as $\phi' = 0$ (see Subsec. III A). We will conduct a detailed study of this case in an upcoming work [56]. We will also constraint the parameter space by performing a numerical fit to cosmological observations in [70].

[1] A. G. Riess *et al.* (Supernova Search Team), Observational evidence from supernovae for an accelerating universe and a cosmological constant, Astron. J. **116**, 1009 (1998), arXiv:astro-ph/9805201.

[2] S. Perlmutter *et al.* (Supernova Cosmology Project), Measurements of Ω and Λ from 42 High Redshift Supernovae, Astrophys. J. **517**, 565 (1999), arXiv:astro-ph/9812133.

[3] N. A. Bahcall, J. P. Ostriker, S. Perlmutter, and P. J. Steinhardt, The Cosmic triangle: Assessing the state of the universe, Science **284**, 1481 (1999), arXiv:astro-ph/9906463.

[4] S. Weinberg, The Cosmological Constant Problem, Rev. Mod. Phys. **61**, 1 (1989).

[5] V. Sahni and A. A. Starobinsky, The Case for a positive cosmological Lambda term, Int. J. Mod. Phys. D **9**, 373 (2000), arXiv:astro-ph/9904398.

[6] S. M. Carroll, The Cosmological constant, Living Rev. Rel. **4**, 1 (2001), arXiv:astro-ph/0004075.

[7] T. Padmanabhan, Cosmological constant: The Weight of the vacuum, Phys. Rept. **380**, 235 (2003), arXiv:hep-th/0212290.

[8] E. Di Valentino, O. Mena, S. Pan, L. Visinelli, W. Yang, A. Melchiorri, D. F. Mota, A. G. Riess, and J. Silk, In the realm of the Hubble tension—a review of solutions, Class. Quant. Grav. **38**, 153001 (2021), arXiv:2103.01183 [astro-ph.CO].

[9] V. Poulin, T. L. Smith, T. Karwal, and M. Kamionkowski, Early Dark Energy Can Resolve The Hubble Tension, Phys. Rev. Lett. **122**, 221301 (2019), arXiv:1811.04083 [astro-ph.CO].

[10] M. Kamionkowski and A. G. Riess, The Hubble Tension and Early Dark Energy, Ann. Rev. Nucl. Part. Sci. **73**, 153 (2023), arXiv:2211.04492 [astro-ph.CO].

[11] E. Di Valentino *et al.*, Cosmology Intertwined III: $f\sigma_8$ and S_8, Astropart. Phys. **131**, 102604 (2021), arXiv:2008.11285 [astro-ph.CO].

[12] L. Perivolaropoulos and F. Skara, Challenges for ΛCDM: An update, New Astron. Rev. **95**, 101659 (2022), arXiv:2105.05208 [astro-ph.CO].

[13] E. Abdalla *et al.*, Cosmology intertwined: A review of the particle physics, astrophysics, and cosmology associated with the cosmological tensions and anomalies, JHEAp **34**, 49 (2022), arXiv:2203.06142 [astro-ph.CO].

[14] J. Lesgourgues and S. Pastor, Massive neutrinos and cosmology, Phys. Rept. **429**, 307 (2006), arXiv:astro-ph/0603494.

[15] S. Hannestad, Primordial neutrinos, Ann. Rev. Nucl. Part. Sci. **56**, 137 (2006), arXiv:hep-ph/0602058.

[16] S. Hannestad, Neutrino physics from precision cosmology, Prog. Part. Nucl. Phys. **65**, 185 (2010), arXiv:1007.0658 [hep-ph].

[17] Y. Y. Y. Wong, Neutrino mass in cosmology: status and prospects, Ann. Rev. Nucl. Part. Sci. **61**, 69 (2011), arXiv:1111.1436 [astro-ph.CO].

[18] J. Lesgourgues and S. Pastor, Neutrino mass from Cosmology, Adv. High Energy Phys. **2012**, 608515 (2012), arXiv:1212.6154 [hep-ph].

[19] V. da Fonseca, T. Barreiro, and N. J. Nunes, Relaxing cosmological constraints on current neutrino masses, Phys. Rev. D **109**, 063517 (2024), arXiv:2311.01803 [astro-ph.CO].

[20] A. Y. Kamenshchik, U. Moschella, and V. Pasquier, An Alternative to quintessence, Phys. Lett. B **511**, 265 (2001), arXiv:gr-qc/0103004.

[21] S. Nojiri, S. D. Odintsov, and S. Tsujikawa, Properties of singularities in (phantom) dark energy universe, Phys. Rev. D **71**, 063004 (2005), arXiv:hep-th/0501025.

[22] I. Albarran, M. Bouhmadi-López, and J. a. Morais, Cosmological perturbations in an effective and genuinely phantom dark energy Universe, Phys. Dark Univ. **16**, 94 (2017), arXiv:1611.00392 [astro-ph.CO].

[23] Y. Akrami *et al.* (CANTATA), *Modified Gravity and Cosmology. An Update by the CANTATA Network*, edited by E. N. Saridakis, R. Lazkoz, V. Salzano, P. Vargas Moniz, S. Capozziello, J. Beltrán Jiménez, M. De Laurentis, and G. J. Olmo (Springer, 2021) arXiv:2105.12582 [gr-qc].

[24] C. Wetterich, Cosmology and the Fate of Dilatation Symmetry, Nucl. Phys. B **302**, 668 (1988), arXiv:1711.03844 [hep-th].

[25] P. G. Ferreira and M. Joyce, Cosmology with a primordial scaling field, Phys. Rev. D **58**, 023503 (1998), arXiv:astro-ph/9711102.

[26] I. Zlatev, L.-M. Wang, and P. J. Steinhardt, Quintessence, cosmic coincidence, and the cosmological constant, Phys. Rev. Lett. **82**, 896 (1999), arXiv:astro-ph/9807002.

[27] P. J. Steinhardt, L.-M. Wang, and I. Zlatev, Cosmological tracking solutions, Phys. Rev. D **59**, 123504 (1999), arXiv:astro-ph/9812313.

[28] C. G. Boiza and M. Bouhmadi-López, Speeding up the Universe with a generalised axion-like potential (2024), arXiv:2409.18184 [astro-ph.CO].

[29] S. C. C. Ng and D. L. Wiltshire, Properties of cosmologies with dynamical pseudo Nambu-Goldstone bosons, Phys. Rev. D **63**, 023503 (2001), arXiv:astro-ph/0004138.

[30] K. Hammer, P. Jirousek, and A. Vikman, Axionic cosmological constant (2020), arXiv:2001.03169 [gr-qc].

[31] D. J. E. Marsh, Axion Cosmology, Phys. Rept. **643**, 1 (2016), arXiv:1510.07633 [astro-ph.CO].

[32] S. Chakraborty, E. González, G. Leon, and B. Wang, Time-averaging axion-like interacting scalar fields mod-

els, Eur. Phys. J. C **81**, 1039 (2021), arXiv:2107.04651 [gr-qc].

[33] M. Kamionkowski, J. Pradler, and D. G. E. Walker, Dark energy from the string axiverse, Phys. Rev. Lett. **113**, 251302 (2014), arXiv:1409.0549 [hep-ph].

[34] R. Emami, D. Grin, J. Pradler, A. Raccanelli, and M. Kamionkowski, Cosmological tests of an axiverse-inspired quintessence field, Phys. Rev. D **93**, 123005 (2016), arXiv:1603.04851 [astro-ph.CO].

[35] K. Freese, J. A. Frieman, and A. V. Olinto, Natural inflation with pseudo - Nambu-Goldstone bosons, Phys. Rev. Lett. **65**, 3233 (1990).

[36] M. Y. Khlopov, S. G. Rubin, and A. S. Sakharov, Primordial structure of massive black hole clusters, Astropart. Phys. **23**, 265 (2005), arXiv:astro-ph/0401532.

[37] M. Y. Khlopov, A. S. Sakharov, and D. D. Sokoloff, The nonlinear modulation of the density distribution in standard axionic CDM and its cosmological impact, Nucl. Phys. B Proc. Suppl. **72**, 105 (1999).

[38] L. Hui, J. P. Ostriker, S. Tremaine, and E. Witten, Ultralight scalars as cosmological dark matter, Phys. Rev. D **95**, 043541 (2017), arXiv:1610.08297 [astro-ph.CO].

[39] H.-Y. Schive, T. Chiueh, and T. Broadhurst, Cosmic Structure as the Quantum Interference of a Coherent Dark Wave, Nature Phys. **10**, 496 (2014), arXiv:1406.6586 [astro-ph.GA].

[40] H.-Y. Schive, M.-H. Liao, T.-P. Woo, S.-K. Wong, T. Chiueh, T. Broadhurst, and W. Y. P. Hwang, Understanding the Core-Halo Relation of Quantum Wave Dark Matter from 3D Simulations, Phys. Rev. Lett. **113**, 261302 (2014), arXiv:1407.7762 [astro-ph.GA].

[41] P. Mocz *et al.*, Galaxy formation with BECDM – II. Cosmic filaments and first galaxies, Mon. Not. Roy. Astron. Soc. **494**, 2027 (2020), arXiv:1911.05746 [astro-ph.CO].

[42] M. W. Hossain and A. Maqsood, Comparison between axionlike and power law potentials in a cosmological background, Phys. Rev. D **109**, 103512 (2024), arXiv:2311.17825 [astro-ph.CO].

[43] V. F. Mukhanov, H. A. Feldman, and R. H. Brandenberger, Theory of cosmological perturbations. Part 1. Classical perturbations. Part 2. Quantum theory of perturbations. Part 3. Extensions, Phys. Rept. **215**, 203 (1992).

[44] C.-P. Ma and E. Bertschinger, Cosmological perturbation theory in the synchronous and conformal Newtonian gauges, Astrophys. J. **455**, 7 (1995), arXiv:astro-ph/9506072.

[45] R. H. Brandenberger, Lectures on the theory of cosmological perturbations, Lect. Notes Phys. **646**, 127 (2004), arXiv:hep-th/0306071.

[46] K. A. Malik and D. Wands, Cosmological perturbations, Phys. Rept. **475**, 1 (2009), arXiv:0809.4944 [astro-ph].

[47] D. Baumann, Cosmology: Part III Mathematical Tripos (Lecture notes).

[48] M. Malquarti and A. R. Liddle, Evolution of large scale perturbations in quintessence models, Phys. Rev. D **66**, 123506 (2002), arXiv:astro-ph/0208562.

[49] B. A. Bassett, S. Tsujikawa, and D. Wands, Inflation dynamics and reheating, Rev. Mod. Phys. **78**, 537 (2006), arXiv:astro-ph/0507632.

[50] A. Wang, D. Wands, and R. Maartens, Scalar field perturbations in Horava-Lifshitz cosmology, JCAP **03**, 013,

arXiv:0909.5167 [hep-th].

[51] S. Weinberg, Adiabatic modes in cosmology, Phys. Rev. D **67**, 123504 (2003), arXiv:astro-ph/0302326.

[52] E. J. Copeland, A. R. Liddle, and D. Wands, Exponential potentials and cosmological scaling solutions, Phys. Rev. D **57**, 4686 (1998), arXiv:gr-qc/9711068.

[53] A. de la Macorra and G. Piccinelli, General scalar fields as quintessence, Phys. Rev. D **61**, 123503 (2000), arXiv:hep-ph/9909459.

[54] S. C. C. Ng, N. J. Nunes, and F. Rosati, Applications of scalar attractor solutions to cosmology, Phys. Rev. D **64**, 083510 (2001), arXiv:astro-ph/0107321.

[55] J. M. Bardeen, Gauge Invariant Cosmological Perturbations, Phys. Rev. D **22**, 1882 (1980).

[56] C. G. Boiza and M. Bouhmadi-López, in preparation.

[57] R. Bean and O. Dore, Probing dark energy perturbations: The Dark energy equation of state and speed of sound as measured by WMAP, Phys. Rev. D **69**, 083503 (2004), arXiv:astro-ph/0307100.

[58] J. Valiviita, E. Majerotto, and R. Maartens, Instability in interacting dark energy and dark matter fluids, JCAP **07**, 020, arXiv:0804.0232 [astro-ph].

[59] E. Pajer and S. Jazayeri, Systematics of Adiabatic Modes: Flat Universes, JCAP **03**, 013, arXiv:1710.02177 [astro-ph.CO].

[60] J. M. Bardeen, P. J. Steinhardt, and M. S. Turner, Spontaneous creation of almost scale-free density perturbations in an inflationary universe, Phys. Rev. D **28**, 679 (1983).

[61] C. Gordon, D. Wands, B. A. Bassett, and R. Maartens, Adiabatic and entropy perturbations from inflation, Phys. Rev. D **63**, 023506 (2000), arXiv:astro-ph/0009131.

[62] G. Ballesteros and J. Lesgourgues, Dark energy with non-adiabatic sound speed: initial conditions and detectability, JCAP **10**, 014, arXiv:1004.5509 [astro-ph.CO].

[63] N. Aghanim *et al.* (Planck), Planck 2018 results. VI. Cosmological parameters, Astron. Astrophys. **641**, A6 (2020), [Erratum: Astron.Astrophys. 652, C4 (2021)], arXiv:1807.06209 [astro-ph.CO].

[64] A. Balcerzak and T. Denkiewicz, Density preturbations in a finite scale factor singularity universe, Phys. Rev. D **86**, 023522 (2012), arXiv:1202.3280 [astro-ph.CO].

[65] L.-M. Wang and P. J. Steinhardt, Cluster abundance constraints on quintessence models, Astrophys. J. **508**, 483 (1998), arXiv:astro-ph/9804015.

[66] E. V. Linder, Cosmic growth history and expansion history, Phys. Rev. D **72**, 043529 (2005), arXiv:astro-ph/0507263.

[67] E. V. Linder and R. N. Cahn, Parameterized Beyond-Einstein Growth, Astropart. Phys. **28**, 481 (2007), arXiv:astro-ph/0701317.

[68] Y. Wang *et al.*, Designing a space-based galaxy redshift survey to probe dark energy, Mon. Not. Roy. Astron. Soc. **409**, 737 (2010), arXiv:1006.3517 [astro-ph.CO].

[69] F. Avila, A. Bernui, A. Bonilla, and R. C. Nunes, Inferring $S_8(z)$ and $\gamma(z)$ with cosmic growth rate measurements using machine learning, Eur. Phys. J. C **82**, 594 (2022), arXiv:2201.07829 [astro-ph.CO].

[70] H.-W. Chiang, C. G. Boiza, and M. Bouhmadi-López, work in progress.